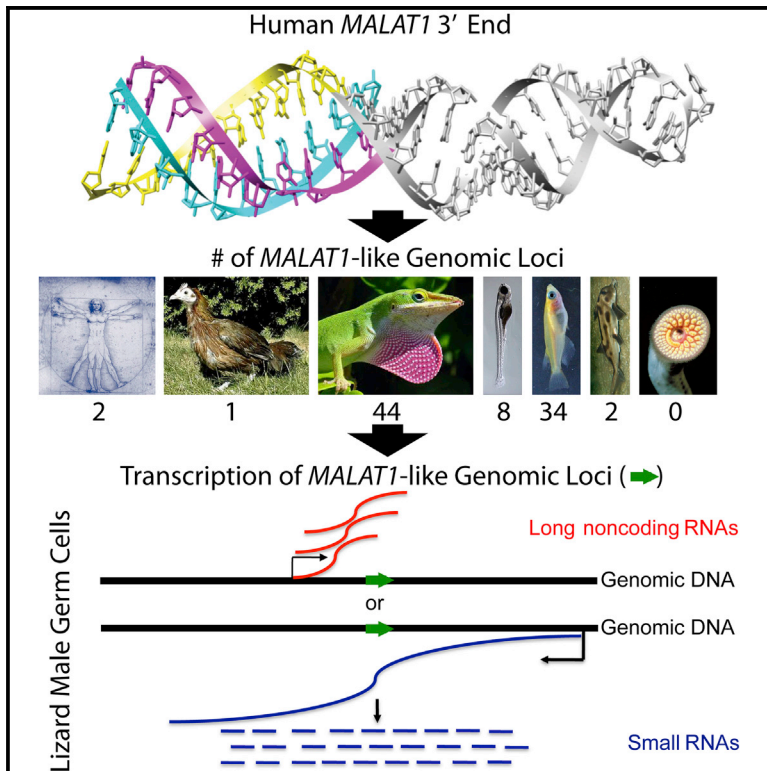


Cell Reports

Identification and Characterization of a Class of *MALAT1*-like Genomic Loci

Graphical Abstract



Authors

Bin Zhang, Yuntao S. Mao,
Sarah D. Diermeier, ..., Sean R. Eddy,
Karissa Y. Sanbonmatsu,
David L. Spector

Correspondence

bin_zhang@urmc.rochester.edu (B.Z.),
spector@cshl.edu (D.L.S.)

In Brief

Zhang et al. find that vertebrate genomes have more than 130 genomic loci with a unique 3' end structure similar to that of *MALAT1*. This class of *MALAT1*-like noncoding RNAs in green lizard is expressed in testis, and it recruits piRNAs derived from the opposite strands to meiotic chromatin in spermatocytes.

Highlights

- The 3' end of *MALAT1*-like RNAs contains triple-helix and tRNA-like structures
- A secondary structure-based covariance model identifies 132 *MALAT1*-like genomic loci
- These genomic loci in lizard express *MALAT1*-like noncoding RNAs and piRNAs
- Lizard long noncoding RNAs recruit the PIWI/piRNA complex to meiotic chromatin

Accession Numbers

GSE97451



Identification and Characterization of a Class of *MALAT1*-like Genomic Loci

Bin Zhang,^{1,2,9,*} Yuntao S. Mao,^{1,9} Sarah D. Diermeier,¹ Irina V. Novikova,^{3,4} Eric P. Nawrocki,^{5,6} Tom A. Jones,⁷ Zsolt Lazar,¹ Chang-Shung Tung,⁴ Weijun Luo,⁸ Sean R. Eddy,⁷ Karissa Y. Sanbonmatsu,⁴ and David L. Spector^{1,10,*}

¹Cold Spring Harbor Laboratory, One Bungtown Road, Cold Spring Harbor, NY 11724, USA

²Department of Pathology and Laboratory Medicine, Department of Pediatrics, University of Rochester Medical Center, 601 Elmwood Avenue, Rochester, NY 14642, USA

³Pacific Northwest National Laboratory, 902 Battelle Boulevard, Richland, WA 99352, USA

⁴Theoretical Biology and Biophysics Group, Los Alamos National Laboratory, MS K710 Los Alamos, NM 87545, USA

⁵Howard Hughes Medical Institute, Janelia Farm Research Campus, Ashburn, VA 20147, USA

⁶National Center for Biotechnology Information, U.S. National Library of Medicine, Bethesda, MD 20894, USA

⁷Howard Hughes Medical Institute, Harvard University, 16 Divinity Avenue, Cambridge, MA 02138, USA

⁸Department of Bioinformatics and Genomics, University of North Carolina at Charlotte, 9201 University City Boulevard, Charlotte, NC 28223, USA

⁹These authors contributed equally

¹⁰Lead Contact

*Correspondence: bin_zhang@urmc.rochester.edu (B.Z.), spector@cshl.edu (D.L.S.)

<http://dx.doi.org/10.1016/j.celrep.2017.05.006>

SUMMARY

The *MALAT1* (Metastasis-Associated Lung Adenocarcinoma Transcript 1) gene encodes a noncoding RNA that is processed into a long nuclear retained transcript (*MALAT1*) and a small cytoplasmic tRNA-like transcript (*mascrRNA*). Using an RNA sequence- and structure-based covariance model, we identified more than 130 genomic loci in vertebrate genomes containing the *MALAT1* 3' end triple-helix structure and its immediate downstream tRNA-like structure, including 44 in the green lizard *Anolis carolinensis*. Structural and computational analyses revealed a co-occurrence of components of the 3' end module. *MALAT1*-like genes in *Anolis carolinensis* are highly expressed in adult testis, thus we named them testis-abundant long noncoding RNAs (tancRNAs). *MALAT1*-like loci also produce multiple small RNA species, including PIWI-interacting RNAs (piRNAs), from the antisense strand. The 3' ends of tancRNAs serve as potential targets for the PIWI-piRNA complex. Thus, we have identified an evolutionarily conserved class of long noncoding RNAs (lncRNAs) with similar structural constraints, post-transcriptional processing, and subcellular localization and a distinct function in spermatocytes.

INTRODUCTION

Long noncoding RNAs (lncRNAs) range in size from 200 nt to >100 kb in length, and they are typically transcribed by RNA polymerase II (Rinn and Chang, 2012). A number of studies

over the past decade, including the Encyclopedia of DNA Elements (ENCODE) project, have identified thousands of lncRNAs, many of which exhibit cell type- and tissue-specific expression, diverse subcellular localization, and disease association (Bertone et al., 2004; Carninci et al., 2005; Derrien et al., 2012; Djebali et al., 2012; Harrow et al., 2012; Kapranov et al., 2007; Katayama et al., 2005; Okazaki et al., 2002). Although some lncRNAs have been shown to act as scaffolds for the assembly of nuclear bodies and cytoplasmic complexes, to play an important role in co-transcriptional gene regulation and chromatin remodeling, or to serve as a molecular decoy to titrate microRNAs (miRNAs) or RNA-binding factors (Chodroff et al., 2010; Guttman et al., 2009; Lee et al., 2016; Mao et al., 2011; Ørom et al., 2010; Rinn et al., 2007; Shevtsov and Dundr, 2011; Ulitsky and Bartel, 2013), the function of the majority of lncRNAs is yet to be determined. In addition, their evolution on both the structural and functional levels and the correlation between structure and function remain largely unclear. As there is a lack of structure-function relationships and sequence conservation among lncRNAs, de novo prediction of lncRNA functional domains is quite challenging (Batista and Chang, 2013).

MALAT1 (Metastasis-Associated Lung Adenocarcinoma Transcript 1) lncRNA, first identified as being upregulated in lung tumors that have the propensity to metastasize (Ji et al., 2003), has subsequently been found to be highly expressed in a large number of tumor types (reviewed in Gutschner et al., 2013a). Unlike most lncRNAs that are expressed at very low levels, *MALAT1* is also highly expressed in many normal tissues (Zhang et al., 2012), and its expression is regulated during development (Bernard et al., 2010; Hutchinson et al., 2007; Ji et al., 2003). Several *Malat1* knockout mouse models have been established, and they exhibit no major phenotype in regard to pre- or post-natal development; they exhibit normal growth and fertility, and *Malat1* deletion does not affect global gene expression or pre-mRNA splicing (Eißmann et al., 2012; Nakagawa et al.,

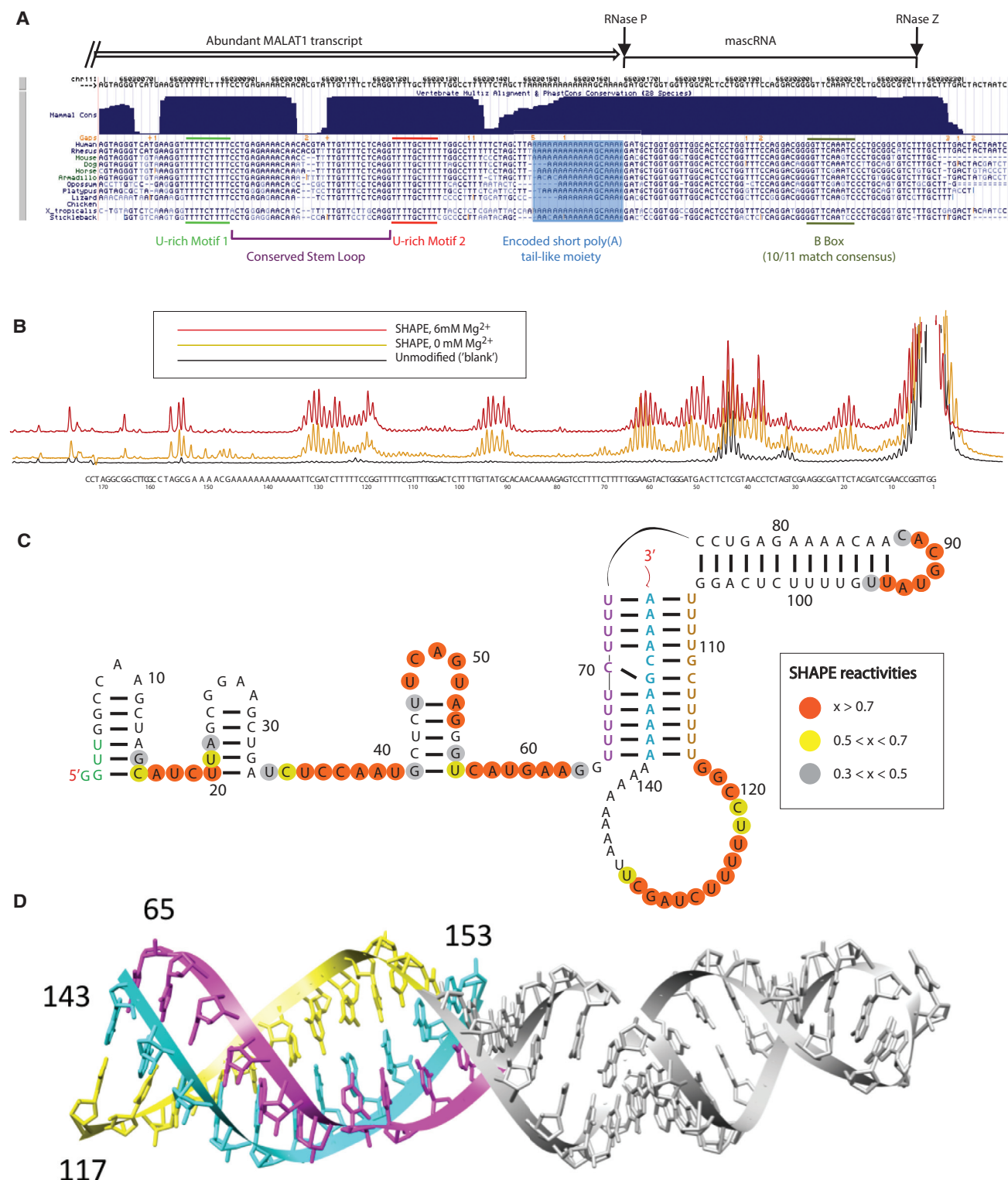


Figure 1. The 3' End of *MALAT1* Forms a Triple-Helix Structure

(A) The sequence conservation of the 3' end of *MALAT1*.

(B) SHAPE chemical probing of the 3' end of human *MALAT1* is consistent with a triple helix. Capillary electrophoresis traces display nucleotides with low and high SHAPE reactivity, corresponding to low and high flexibility. Black, unmodified control; gold, SHAPE reactivity for 0 mM Mg^{2+} ; red, SHAPE reactivity for 6 mM Mg^{2+} .

(legend continued on next page)

2012; Zhang et al., 2012). The lack of phenotype upon the in vivo loss of *Malat1* lncRNA transcripts could be attributed to functional redundancy with other RNA transcripts or to its subtle cellular and developmental function, which may be compensated or manifest phenotypes only under certain physiological conditions, as occurs with respect to many protein-coding genes (Zhang et al., 2012). Interestingly, knockdown of *MALAT1* in several cultured cell lines results in altered pre-mRNA splicing (Tripathi et al., 2010) or E2F1-regulated cell-cycle progression (Yang et al., 2011). In addition, two genome-wide studies have indicated that *MALAT1* binds to transcription start sites (TSSs) and to gene bodies of actively transcribing genes together with lncRNA *NEAT1* (West et al., 2014) and to nascent pre-mRNAs indirectly via protein partners (Engreitz et al., 2014). Notably, human lung tumor cells lacking *MALAT1* are impaired in cell migration, and they are unable to efficiently develop tumor nodules in a mouse xenograft model (Gutschner et al., 2013b). Furthermore, genetic knockout or antisense oligonucleotide (ASO)-mediated knockdown of *Malat1* in vivo in a mouse mammary tumor model results in the differentiation of mammary tumors and significant reduction of metastasis (Arun et al., 2016), supporting a context-dependent function of *Malat1*.

MALAT1 nascent transcripts are processed by RNases P and Z to produce a long nuclear-retained ncRNA with a 3' end genetically encoded short polyA-like tail and a 58-nt small tRNA-like cytoplasmic RNA (*masrcRNA*) (Wilusz et al., 2008). Secondary and tertiary structures of lncRNAs have been shown to regulate RNA stability and function through different molecular mechanisms. For example, the stability of polyadenylated nuclear (PAN) RNA produced by Kaposi's sarcoma-associated herpesvirus is regulated by a nuclear retention element for nuclear expression (ENE) near its 3' end that forms a triple-helix structure to prevent 3' nuclease cleavage (Brown et al., 2012). Recently, the 3' ends of *MALAT1* and *Menβ* (*Neat1*) lncRNAs have also been shown to form a triple-helix structure, which functions to stabilize the RNA (Brown et al., 2012, 2014; Wilusz et al., 2012). Evolution of the *MALAT1* gene has been examined, but its origin and function remain largely elusive (Pauli et al., 2012; Stadler, 2010; Ulitsky et al., 2011).

Here we analyzed the secondary and tertiary structures of the 3' end region of *MALAT1* lncRNA from multiple species using a chemical probing approach. Our results are consistent with a triple-helix complex upstream of the RNase P cleavage site. Using computational modeling based on this identified secondary RNA structure, 132 genomic loci resembling the *MALAT1* 3' end processing module have been identified among several vertebrate genomes, including 44 in the lizard *Anolis carolinensis*. Molecular genomic analyses show that *MALAT1* is highly conserved during evolution in terms of its length, expression, and subcellular localization. Despite a lack of significant sequence similarity among the 5' regions of *MALAT1* in vertebrates, a high degree of RNA structural conservation is observed in its 3' end among human, zebrafish, and lizard, implicating critical molecular and/or cellular

functions of the *MALAT1* 3' end. *MALAT1*-like genes in *Anolis carolinensis* do not appear to encode proteins and are highly expressed in testis, and, as such, we have named them testis-abundant long noncoding RNAs (*tancRNAs*). Surprisingly, molecular characterization has identified multiple small RNA species derived from *tancRNA* loci, including PIWI-interacting RNAs (piRNAs) from the antisense strand. Interactions between lizard PIWI proteins and *tancRNAs*, along with sequence complementation between *tancRNAs* and their associated piRNAs, implicate the coevolved 3' structure complex of *tancRNAs* to act as potential targets for the PIWI-piRNA complex. In summary, we define a class of lncRNAs with a conserved structural complex, post-transcriptional processing, and subcellular localization, and we demonstrate a function for these RNAs and/or genomic loci in green lizard spermatocytes.

RESULTS

The 3' End of *MALAT1* Forms a Triple-Helix Structure and a tRNA-like Structure

Although present from fish to human, *MALAT1*'s primary sequence conservation is predominantly constrained to its 3' end, which comprises two highly conserved U-rich regions followed by a conserved A-rich tract upstream of the RNase P cleavage site. A tRNA-like *masrcRNA* is encoded downstream of the A-rich tract (Figure 1A; Wilusz et al., 2008). To experimentally probe the structure of the 3' end of *MALAT1*, we performed SHAPE (selective 2'-hydroxyl acylation analyzed by primer extension) and DMS (dimethyl sulfate) analyses on the human, lizard, and zebrafish *MALAT1* 3' ends. Low SHAPE reactivities are consistent with relatively low mobility of the backbone of a nucleotide (specifically the 2'-hydroxyl group). This occurs when the nucleotide participates in a base pair or a highly stable tertiary structure, such as a triple-helix configuration. Low DMS reactivities occur when a nucleotide is protected by interactions, such as base-pairing interactions or participation in a triple-helix conformation.

Raw probing traces were obtained via capillary electrophoresis for all RNAs studied (Figure 1B; Figures S1 and S2). In all three RNAs, we observed significant protection of the U-rich and A-rich sequences against SHAPE and DMS reagents, consistent with the formation of a conserved triplex architecture, where U-A-U base triples represent the major organizing motif, intervened by a C-G-C base triplet (Figure 1C; Figures S1 and S2). The human and zebrafish triplexes contain ten base triples. The lizard *MALAT1* structures only contain nine Watson-Crick base triples; however, this structure contains a G-A-C motif on the end of the triplex adjacent to the loop. The G-A-C motif can also form a base triple, as observed in the nuclear magnetic resonance (NMR) structure of the aptamer domain of the pre-quosine (preQ) riboswitch (Kang et al., 2014). Each of the three structures also contains a conserved stem-loop. This helix protrudes from the triplex and is capped by a small tetraloop or

(C) Secondary structure of the 3' end of human *MALAT1*, as inferred by SHAPE and DMS probing experiments (data not shown). Orange, high reactivity; yellow, medium reactivity; gray, low reactivity; un-circled nucleotides, near-zero reactivity.

(D) Tertiary structure model of the 3' end of human *MALAT1* demonstrates stereochemical feasibility of a triple helix. Purple, yellow, and cyan strands correspond to similarly colored strands in (C).

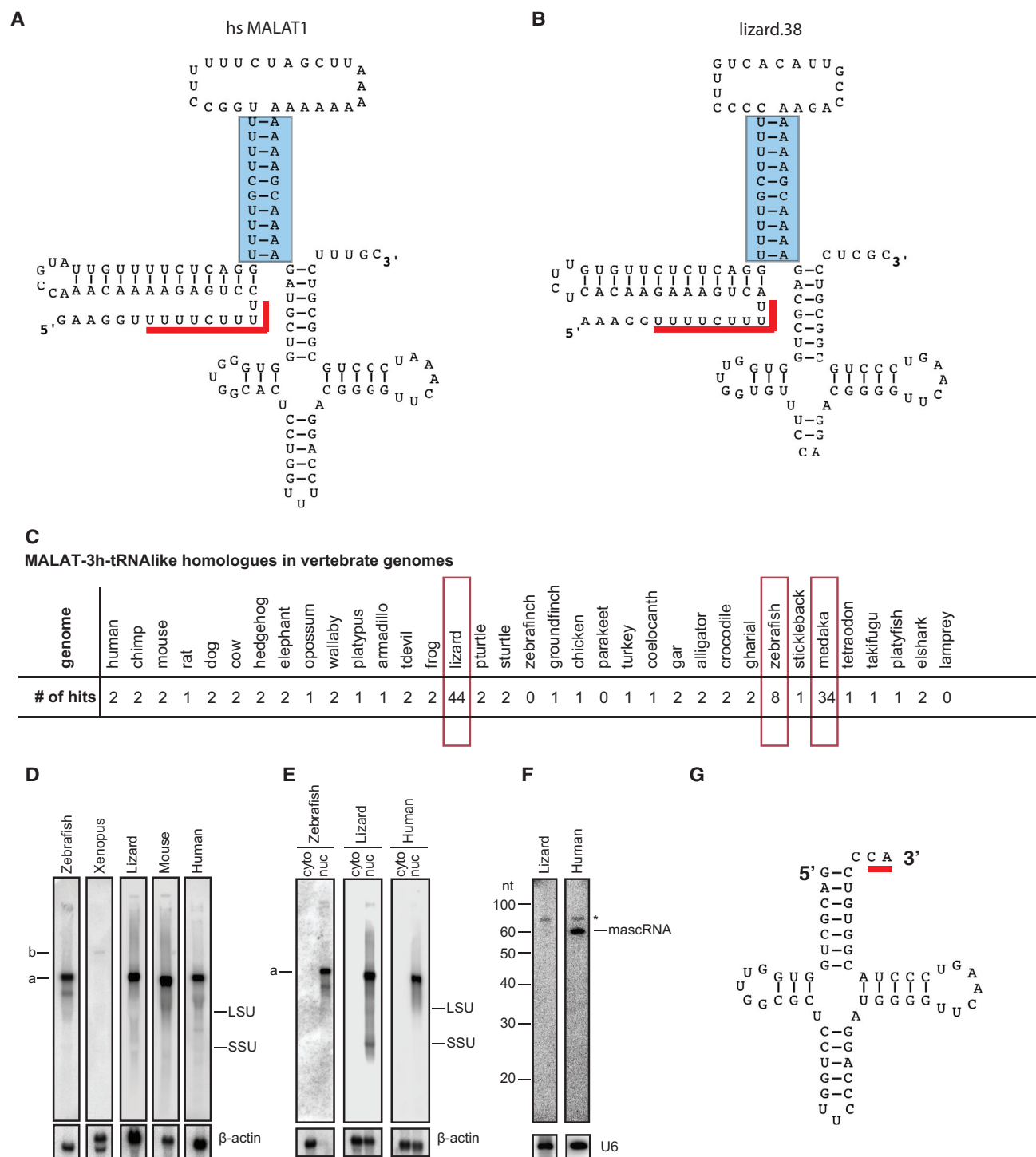


Figure 2. A Class of Genomic Loci with Structures Similar to the MALAT1 3' End Was Identified in Vertebrate Genomes

(A) The primary sequence and predicted secondary structure of human MALAT1 3' module, as identified by a homology search using Infernal 1.1rc1 against the human genome using CM file MALAT1-3h-tRNAlike.cm (Data S1). Only base pairs modeled by the CM are indicated with lines connecting two nucleotides. The triple helix is formed between the stem structure indicated by a blue rectangle and its upstream U-rich motif indicated by a red line.

(B) One MALAT1 3' end homolog (lizard.38) with a degenerative tRNA-like structure that was identified in the lizard genome using the MALAT1-3h-tRNAlike.cm CM profile.

(C) Summary of MALAT1-3h-tRNAlike hits with an E value less than 1×10^{-11} in 35 genomes (see Data S1). Note that most mammals have one or two hits, while lizard, zebrafish, and medaka have more than two MALAT1-3h-tRNAlike hits (highlighted in red open rectangles).

(legend continued on next page)

pentaloop, depending on the RNA. Using previously developed RNA homology techniques (Budkevich et al., 2014; Tung et al., 2002), we constructed 3D models of the triplex tertiary structures (Figure 1D). The triplex structures contain base triples consisting of various combinations of A and U or various combinations of G and C, along with a stem-loop containing a large number of purine bases. These are all features observed in the triple helix revealed by crystallographic studies of the SAM-II riboswitch aptamer domain (Gilbert et al., 2008). The long stem-loop easily stacks onto the triple helix while maintaining reasonable stereochemistry.

In contrast to the highly conserved triplexes, the regions of RNA preceding the triplexes (5' ends) are highly reactive and vary significantly with respect to each other (data not shown). The human *MALAT1* 3' end contains three consecutive stem-loops connected by highly reactive and likely flexible stretches of RNA. The zebrafish *MALAT1* 3' end contains a single stem-loop surrounded entirely by flexible bases, as does the lizard *MALAT1* 3' end (Figure S2).

We also performed SHAPE and DMS analyses on the human *malacRNA*, and we observed significant protection of the predicted stem structures against SHAPE and DMS reagents, consistent with the formation of a conserved cloverleaf architecture (Figure S3).

A Class of Genomic Loci with Structures Similar to the *MALAT1* 3' End Is Present in Vertebrate Genomes

Given the presence of an unusual 3' end structure (triple helix and tRNA-like RNA) associated with a unique processing mechanism of the *MALAT1* lncRNA that is conserved from fish to human, we hypothesized that this structure and mechanism may exist in other lncRNAs or mRNAs. To search for RNA molecules containing these domains, we built a covariance model (CM) profile (MALAT1-3h-tRNAlike.cm in Data S1), using Infernal (Nawrocki and Eddy, 2013) based on structures determined by chemical probing analysis described above (Figure 2A). We identified 132 hits in 35 vertebrate genomes (genome version information in Data S1) with an E value less than 10^{-11} (Figures 2A–2C; Data S1). Based on the low E values, we were confident that all or nearly all of these hits were homologous to the *MALAT1* 3' end. However, some hits, particularly in the Medaka genome, had multiple mutations that disrupted the proposed secondary structure, indicating that the structure was no longer being conserved in those cases.

Although *MALAT1* 3' end homologs were not found in jawless vertebrates or in any non-vertebrates examined, one or two *MALAT1*-like genomic loci were identified in most genomes except for zebra finch and parakeet (Figure 2C). Searches with BLAST as well as with Infernal using a model built only from the turkey hit found no homologs in the zebra finch and parakeet genomes. We suspect that this may be due to incomplete coverage

of those genome sequences. The elephant shark is the most distant organism from human in which we identified potential homologs of the *MALAT1* triple-helix and tRNA-like structures.

The two genes identified in most vertebrate genomes are homologs of the human *MALAT1* and *NEAT1* genes. These two adjacent lncRNAs with similar 3' end structures likely represent a genomic duplication during evolution. In *Xenopus*, these two lncRNAs are oriented in a transcriptionally convergent fashion, which could represent another independent gene duplication event. Interestingly, a significantly greater number of hits were identified in the genomes of lizard (44 hits), zebrafish (8 hits), and medaka (34 hits), suggesting potential expansions of this element in these organisms. Taken together, our results suggest that it is likely that the *MALAT1* 3' end triplex and tRNA-like structure complex existed in the common ancestor of cartilaginous fish and mammals, and it has been maintained through evolution with gene duplication and lineage-specific expansions.

To test whether the triple-helix structure and tRNA-like structure ever occur separately in genomes, we built CM profiles for the triple-helix (MALAT1-3h.cm in Data S1) and tRNA-like regions (MALAT1-tRNAlike.cm in Data S1), separately, and we searched the genomes for homologs. In general, whenever there was a high-scoring hit to either the triple-helix or tRNA-like region, these hits were adjacent and so a high-scoring hit to the combined model (MALAT1-3h-tRNAlike.cm in Data S1) also existed. The main exceptions were in medaka, zebrafish, and one case in lizard. The consistency of the hits among the three models (MALAT1-3h-tRNAlike.cm, MALAT1-3h.cm, and MALAT1-tRNAlike.cm, summarized in Data S1) suggests that the *MALAT1* 3' end triple-helix and tRNA-like structures co-occurred.

MALAT1 Is Highly Expressed in Vertebrates

To determine if *MALAT1* orthologs in lizard, *Xenopus*, and zebrafish are expressed, we performed northern blot analysis using RNAs extracted from cell lines of each species (Figure 2D). Lizard *MALAT1* and zebrafish *MALAT1* were expressed at high levels in IgH-2 (lizard) and ZFL (zebrafish) cells, respectively, and they exhibited a similar size (~7 knt) to human and mouse *MALAT1* in U2OS and NIH 3T3 cells, respectively. *Xenopus MALAT1* was ~11 knt in length and expressed at a relatively lower level in *Xenopus* A6 cells. Similar to human and mouse, lizard and zebrafish *MALAT1* were also enriched in the cell nucleus (Figure 2E). Human and mouse *MALAT1* were specifically localized to nuclear speckles, where nuclear splicing factors are enriched (Bernard et al., 2010; Hutchinson et al., 2007). RNA fluorescence in situ hybridization (FISH) analysis of lizard *MALAT1* in kidney and IgH-2 cells showed a punctate labeling pattern in nuclei (Figure S4; data not shown for IgH-2 cells); however, whether these domains directly corresponded to nuclear speckles in lizard cells was not directly tested.

(D) Northern blot analysis shows that *MALAT1* orthologs were expressed from cultured cells of zebrafish (ZFL), *Xenopus* (A6), lizard (IgH-2), mouse (C2C12), and human (U2OS).

(E) Northern blot analysis shows that *MALAT1* is enriched in nuclei of cultured cells of zebrafish (ZFL), lizard (IgH-2), and human (U2OS).

(F) Small RNA northern blot analysis shows that lizard *malacRNA* is not detectable in the IgH-2 cell line.

(G) Secondary structure of lizard *malacRNA* in the IgH-2 cell line with noncanonical CA tail modification indicated by a red line. β -actin and U6 are loading controls. LSU, large subunit of ribosomal RNA; SSU, small subunit of ribosomal RNA; cyto, cytoplasmic fraction; nuc, nuclear fraction; *non-specific band.

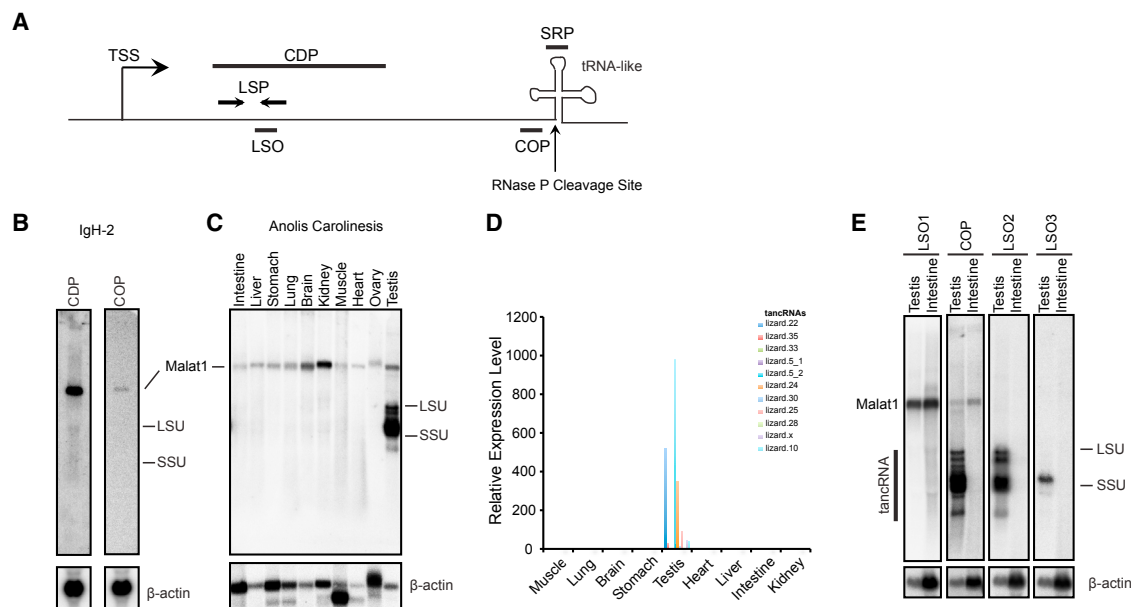


Figure 3. Long Noncoding RNAs Are Produced from *MALAT1*-like Genomic Loci in *Anolis carolinensis* in a Tissue-Specific Manner

(A) Schematic of the transcriptional unit of the *Malat1* 3' module homologous loci. TSS, transcription start site; CDP, IgH-2 cDNA probe (used in B); COP, consensus oligonucleotide probe that is derived from the multi-sequence alignment of 44 homologs (used in B, C, and E); LSP, locus-specific primer (used in D); LSO, locus-specific oligonucleotide (used in E); SRP, small RNA probe; the vertical arrow, the predicted RNase P cleavage site just before the tRNA-like structure.

(B) Northern blot analysis shows that *MALAT1* RNA is highly expressed in lizard IgH-2 cells detected by both cDNA probe and COP, but no other RNA species is detected by the COP.

(C) Northern blot analysis shows that COP labels *MALAT1* in all tissues of *Anolis carolinensis* and multiple RNA species in testis (named tancRNAs).

(D) The qRT-PCR analysis using locus-specific primer (LSP) sets shows that tancRNAs from different genomic loci are specifically expressed in lizard testis. y axis, relative expression level; x axis, different tissues.

(E) Northern blot analysis shows that tancRNAs are expressed from different genomic loci. Note that LSO1 recognizes *MALAT1*, LSO2 recognizes multiple tancRNA species (lizard.20, lizard.12, and lizard.8), and LSO3 detects one major tancRNA species (lizard.30). β -actin is the loading control.

Surprisingly, we did not detect *mascrRNA* in lizard IgH-2 cells by northern blot analysis (Figure 2F), despite high expression of *MALAT1* lncRNA. We hypothesized that lizard *mascrRNA* may be unstable, as previously suggested for men (*NEAT1*)-associated small cytoplasmic RNA (menRNA) in some cell types (Wilusz et al., 2011). However, using a more sensitive PCR-based method, we were able to clone and sequence *mascrRNA* from IgH-2 cells, and we found that lizard *mascrRNA* has a noncanonical 3' tail modification (Figure 2G; Figure S5). Eight clones contained a classical CCA tail addition, while 21 clones contained a truncated CA tail addition. Atypical 3' CCACCA addition to *menRNA* has been reported to impact *menRNA* stability (Kuhn et al., 2015; Wilusz et al., 2011), but it remains to be determined if these noncanonical 3' modifications are a cause or a consequence of RNA stability. It is noted that the 3' first non-paired discriminator base of lizard *mascrRNA* is cytosine (C), which may impact its stability, as the discriminator base contributes significantly to the stem structure and stability of the duplex, and cytosine is the least frequent discriminator nucleotide observed at position 73 of tRNA sequences (Limmer et al., 1993). In addition, how lizard CCA-adding enzyme is able to only add CA to a tRNA-like structure remains to be investigated. Taken together, *MALAT1* lncRNA is highly expressed and enriched

in the nucleus in lower organisms, while the tRNA-like *mascrRNA* is not stable when it contains a noncanonical 3' tail modification in lizard.

A Class of Long Noncoding RNAs Is Produced from *MALAT1*-like Genomic Loci in *Anolis carolinensis* in a Tissue-Specific Manner

To determine if *MALAT1*-like genomic loci are transcriptionally active, we performed northern blot analysis, using a *MALAT1* cDNA probe and consensus oligonucleotide probe (COP) upstream of the RNase P cleavage site, to probe RNAs isolated from IgH-2 cells, and we detected a single RNA species with the expected size of *MALAT1* (Figure 3B). Northern blot analysis on different tissues of *Anolis carolinensis* detected the expression of *MALAT1* in all tissues examined, while expression of a family of RNA species with different sizes was predominantly present in testis (Figure 3C).

To distinguish if these different-sized RNA species are transcripts from different *MALAT1*-like loci or are processed products of abundant *MALAT1*, we performed loci-specific qRT-PCR, and we detected a significant amount of transcripts from upstream regions of multiple *MALAT1*-like loci (Figure 3D). Using probes recognizing specific *MALAT1*-like loci, we detected specific RNA species (Figure 3E).

As these RNA species may not have canonical poly-adenosine tails, not-so-random sequencing (NSR-seq) using not-so-random primer sets was performed on both lizard testis and brain mRNAs to obtain full-length, strand-specific profiles of non-ribosomal RNA transcripts independent of their 3' tail status (Armour et al., 2009; Experimental Procedures). Reads from testis (13.6 million) and brain (15.6 million) were mapped to the lizard genome. Consistent with the results from northern blot analysis, NSR-seq analysis revealed a high expression of *MALAT1* in both brain (data not shown) and testis (Figure 4F), and, in contrast, transcripts from different *MALAT1* 3' end-like genomic loci were specifically expressed in testis (Figures 4A–4E). Most transcripts, including *MALAT1*, were derived from the same strand as the orientation of *MALAT1* 3' end-like elements, which typically sat at their 3' ends as indicated by an apparent drop of downstream read coverage (lizard.2, lizard.3, lizard.5, lizard.15, and lizard.21 in Figures 4A–4D and 4F). This supports the idea that *MALAT1* 3' end-like elements serve as a 3' end RNA module for processing, stabilization, and/or other functions.

These transcripts did not contain potential open reading frames (ORFs) longer than 100 amino acids. Since multiple *MALAT1*-like loci were highly transcribed in lizard testis, we named these transcripts tancRNAs. Size heterogeneity of tancRNA species likely comes from divergent sequences, different promoters, and unique transcription initiation sites upstream of each *MALAT1* 3' end-like module. Future investigation will shed insights into how this novel class of RNA species is regulated and evolved at a molecular level.

Interestingly, some transcripts, such as that from the lizard.37 locus, appeared to be expressed from the opposite strand with a relatively low read coverage and to have the *MALAT1* 3' end-like element in the middle (Figure 4E). These may represent a different RNA species from that described above, and they may have a role in tancRNA regulation.

Multiple Small RNA Species Are Produced from TancRNA Loci

To study the post-transcriptional processing of these RNAs, northern blot analysis was performed using oligonucleotide probes that hybridized to the triple-helix (COP), the tRNA-like structure (small RNA probe [SRP]) (Figure 5B), and a region immediately downstream of the tRNA-like structure (data not shown). Both *MALAT1* and tancRNAs in lizard testis ended just upstream of the predicted RNase P cleavage site, indicating that nascent tancRNA transcripts are processed by the tRNA-processing machinery similar to the processing of human *MALAT1* (Figure 5B). A very light smear was noted in testis, suggestive of an incomplete cleavage. This was also supported by noticeable NSR-seq read coverage downstream of the tRNA-like structure (Figures 4A–4D). The structural analysis of the 3' end of tancRNAs revealed a similar structural complex with a triplex structure associated with a stem-loop, as defined in human *MALAT1* (Figure S6).

We refer to the small RNAs associated with the processing of *MALAT1*-like transcripts as tancRNA-associated small cytoplasmic RNAs (tascRNAs). Northern blots for small RNAs using a consensus probe detected a band with a size of ~60 nt, corre-

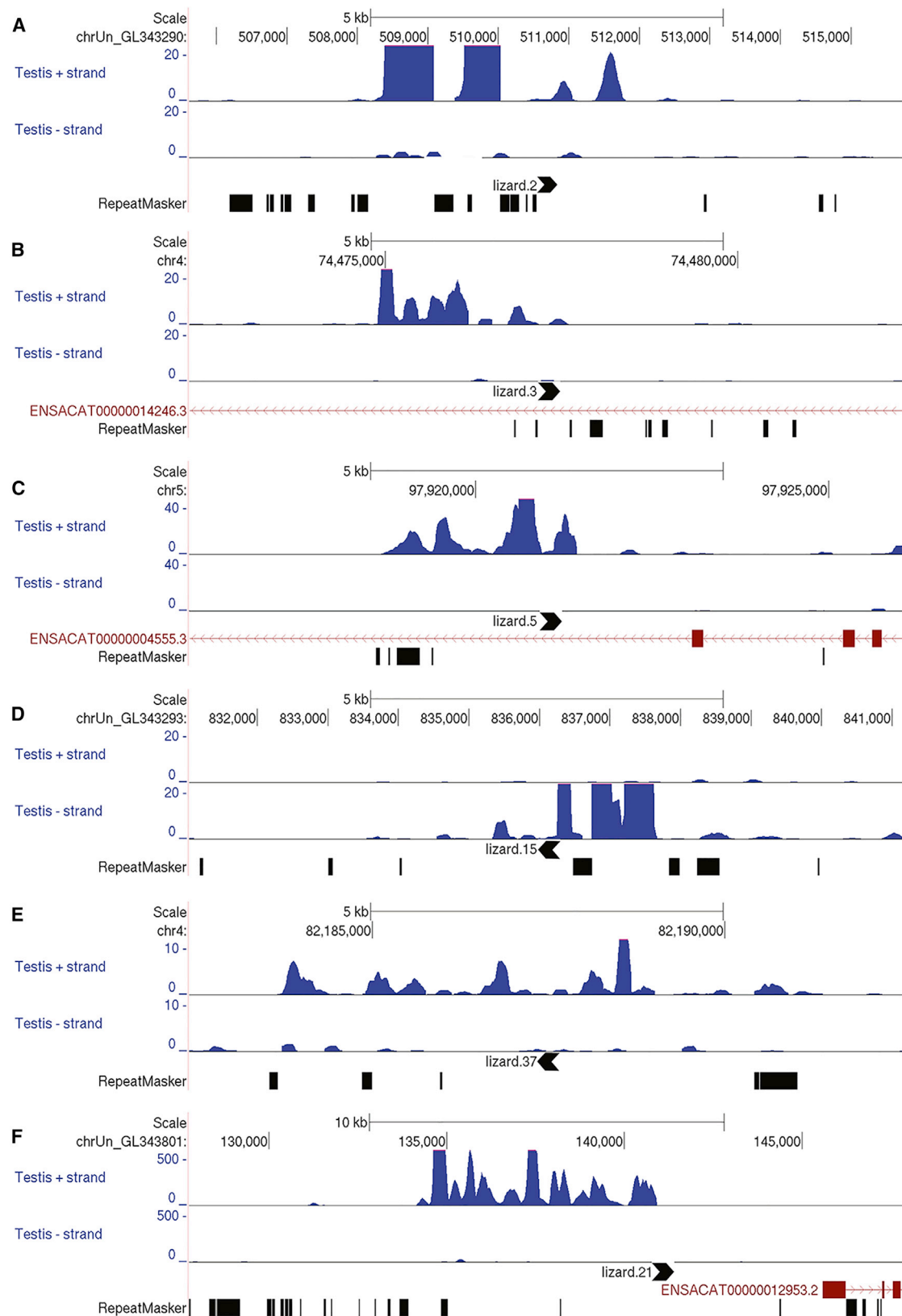
sponding to *mascrRNA* and/or *tascRNAs* (Figure 4C) enriched in testis. The *mascrRNA* was not detectable in intestine, which was consistent with the finding that *mascrRNA* is unstable in the lizard cell line (Figure 2F). Northern analysis using ~200-bp DNA fragments from five tancRNA loci containing the triple-helix and tRNA-like structures also detected the *tascRNA*, but, surprisingly it identified two additional RNA species (sRNA1 and sRNA2) with sizes around 45 and 28 nt, respectively (Figure 5C). The ~28-nt small RNAs were the most abundant among the three RNA species. To further test if the region upstream of the RNase P cleavage site contributes to the production of the abundant sRNA1, we performed 5' rapid amplification of cDNA ends (RACE), and we determined the 5' end of one tancRNA and cloned a full-length cDNA, named tancRNA.11 (chr5:105,700,153–105,702,202) from the lizard.11 locus (Figure S7). This transcriptional unit was also supported by NSR-seq analysis (data not shown). Northern analysis using a tancRNA.11 cDNA probe detected the abundant sRNA1, while sRNA2 and *tascRNAs* were not detected (Figure 5D). These results demonstrated that the processing of the 3' end triple-helix and tRNA-like structure complex is retained in lizard tancRNAs and that multiple small RNA species are generated from tancRNA loci.

TancRNAs Are Enriched in the Nuclei of Round Spermatocytes

To determine what cell types express tancRNAs, we performed RNA FISH using cDNA probes for *Malat1* and tancRNA on adult lizard testicular frozen sections. The developmental stage of adult lizard testis was assessed by SYCP3 staining, showing the presence of pachytene nuclei (data not shown). Interestingly, *Malat1* was highly expressed in cells localized at the periphery of seminiferous tubules and enriched in a punctuate nuclear distribution (Figure 5F), while tancRNAs (detected by the lizard.11 cDNA probe that recognizes the 3' end module, which is shared by all tancRNA loci and the upstream sequence of five tancRNA loci) were highly expressed in differentiating germ cells located in the middle portion of seminiferous tubules, consistent with the location of pachytene and round spermatocytes, and also enriched in nuclei with a punctuate staining pattern (Figure 5E). While the tancRNA cDNA probe could theoretically also detect small RNAs produced from the same locus, the majority of signals were likely derived from lncRNAs, as a similar RNA FISH pattern was observed using an oligonucleotide probe that recognizes tancRNAs (data not shown). Super-resolution imaging using the optical microscope experimental (OMX) microscope demonstrated that tancRNA molecules were dispersed throughout the entire nuclei with an enrichment in interchromatin spaces (Figure 5G). These data indicate that tancRNAs are nuclear lncRNAs in pachytene spermatocytes.

TancRNA Loci Produce piRNAs from Their Antisense Strand

The sRNA1 produced from tancRNA loci has a similar size to piRNAs specifically expressed in germ cells and associated somatic cells (Aravin and Hannon, 2008). Given the expression pattern of sRNA1 and related tancRNAs, we hypothesized that sRNA1 could represent a type of lizard piRNA and sRNA2 the



(legend on next page)

intermediate product. To test this possibility, we performed RNA sequencing (RNA-seq) for small RNAs with the size ranges from 19 to 33 nt (19.0 million reads) and 52 to 68 nt (24.6 million reads). RNA molecules with sizes from 24 to 33 nt exhibited classical features of piRNAs, including 5' U bias (Figure 6A). Interestingly, we noticed a significant 10A bias in the whole population of sRNA1 (Figure 6A). When filtering out 1U RNA molecules, the 10A bias became more prominent (data not shown). This suggests that there may be a ping-pong amplification signature in lizard pachytene piRNAs.

More than 94% of small RNAs with sizes ranging from 24 to 33 nt were successfully mapped to the lizard genome (version anoCar2.0). Small RNAs with sizes ranging from 52 to 68 nt had a similar distribution along the lizard genome, indicating that these molecules are likely the intermediate products of piRNA biogenesis. A total of 763 piRNA clusters were identified with 30 unique small RNA species per kilobase. The average size of these clusters was 9.4 kb. A number of dual-strand overlapping piRNA clusters were identified. For example, the piRNA cluster at chrLGb:2,125,001–2,136,000 was ~11 kb in length, with a strong piRNA production from the positive strand (336,088 reads collapsed into 4,950 unique RNA species) and a relative weaker production from the negative strand (7,522 reads collapsed into 1,460 unique RNA species) (Figure 6B). Analysis of overlapping pairs demonstrated a strong peak for 10-nt overlap, indicating ping-pong amplification for this cluster (Figure 6C). This is a rather unexpected finding since a ping-pong signature has not been reported in non-transposon-derived pachytene piRNAs (Beyret et al., 2012), suggesting that lizard pachytene piRNA biogenesis and action may be different from those in mammalian species or that lizard pachytene piRNAs have a stronger ping-pong signature than their mammalian counterparts.

Eleven tancRNA loci overlap with piRNA clusters ($p < 0.001$; $P[E] = 0.20\%$ and $P[O] = 22.45\%$). Three prominent piRNA clusters (size, >15 kb; piRNA density, >80 unique small RNA species per kilobase), chr2:120,609,001–120,674,000, chr4:82,182,473–82,194,005, and chrUn_GL343674:2,001–17,000, were identified and overlapping with tancRNA loci (lizard.40, lizard.37, and lizard.33, respectively). The piRNAs were only produced from the antisense strand relative to the orientation of tancRNAs or the triple-helix and tRNA-like complex (Figure 6D). This was not a random event, and it was statistically significant that three of 44 tancRNA loci produced piRNAs from the antisense strand ($p < 0.001$), consistent with the strand orientation of long transcripts from these loci (Figure 4E). Because of primary sequence similarity, many piRNAs produced from three clusters can recognize tancRNAs with the triple-helix and tRNA-like structures from different genomic loci. In contrast, the remaining eight tancRNA-associated piRNA clusters were shorter in size (average 8 kb)

with a much lower piRNA density (average 51 piRNA/kb), among which three were from the same strand while five were from the opposite strand of tancRNAs. In addition, there were tancRNA loci that did not overlap with piRNA clusters but could be recognized by piRNAs likely produced from other tancRNA loci in the genome. For example, there were 5,137 small RNA-seq reads mapped to the locus at chrUn_GL343290:510,550–510,800, which actively produces tancRNA (lizard.2; Figure 6E). These results indicate that piRNAs recognize tancRNA 3' ends, but they do not appear to mediate targeted RNA cleavage (Figure 6E), suggesting a unique mechanism(s) of action for these piRNAs and tancRNAs.

One possibility is that tancRNAs may serve as nuclear targets of the PIWI-piRNA complex. To investigate this, we performed computational analysis of the PIWI protein family in lizard, and we found that there are four PIWI homologs, LIWI1a, LIWI1b, LIWI2, and LILI, in lizard (Figure S8). All four PIWI homologs were expressed at a relatively high level in testis and ovary at the RNA level (Figure S8), while LIWI2 protein was only detected in testis (Figure S8). Interestingly, LIWI2 carries a variant residue S at the third residue of the conserved catalytic triad DDH (Song et al., 2004), and it is predicted to be enzymatically inactive (Figure 7B). Chromatin RNA immunoprecipitation (ChRIP) analysis showed that LIWI2 protein is associated with tancRNAs (Figure 7C), and also it demonstrated that tancRNAs are associated with chromatin (Figure 7A). Taken together, piRNAs produced from the antisense strand are able to recognize tancRNAs through the 3' end triple-helix/tRNA-like structure complex, and they potentially direct the enzymatically inactive LIWI2 protein complexes to chromatin in *cis*, via nascent tancRNA transcription, and/or in *trans*, mediated by 5' tancRNA-associated RNA-chromatin interaction (Figure 7D). The proposed in *cis* mechanism is analogous to the PIWI-piRNA-pit-RNA-mediated sequence-specific methylation of an imprinted mouse locus (Watanabe et al., 2011). The in *trans* mechanism likely has a profound impact on chromatin remodeling and genome-wide expression during the development of pachytene spermatocytes in lizard, representing a potential mode of action of non-transposon-derived pachytene piRNAs in human and mouse as well, and thus it warrants further investigation.

DISCUSSION

The recent discovery of lncRNAs in different species and their implicated potential roles in a variety of cellular and molecular processes demand a systematic classification of these species of RNA molecules based on their intrinsic properties. However, weak primary sequence conservation makes it a rather challenging task. We analyzed the secondary and tertiary RNA structures of the 3' end of *MALAT1* lncRNA, and we identified a family

Figure 4. Different Examples of Transcripts from *MALAT1*-like Genomic Loci

(A–F) Transcriptional characteristics of the following *MALAT1*-3h-tRNAlike loci: lizard.2 (A), lizard.3 (B), lizard.5 (C), lizard.15 (D), lizard.37 (E), lizard.21 (F) (*MALAT1* orthologue). Predominant transcripts are derived from the same strand as the *MALAT1*-3h-tRNAlike element at lizard.2, lizard.3, lizard.5, lizard.15, and lizard.21 (A)–(D) and (F), while from the opposite strand at lizard.37 (E). Normalized RNA-seq reads from testis (upper track, reads on sense strand; lower track, reads on antisense strand). Black arrowheads denote *MALAT1*-3h-tRNAlike loci and their direction of transcription. Chromosome location and annotated Ensembl transcripts are indicated. Read depth scale is displayed on the y axis. Interspersed repeats and low-complexity DNA sequences are indicated in the RepeatMasker track. Six examples are shown (nomenclature according to Data S1).

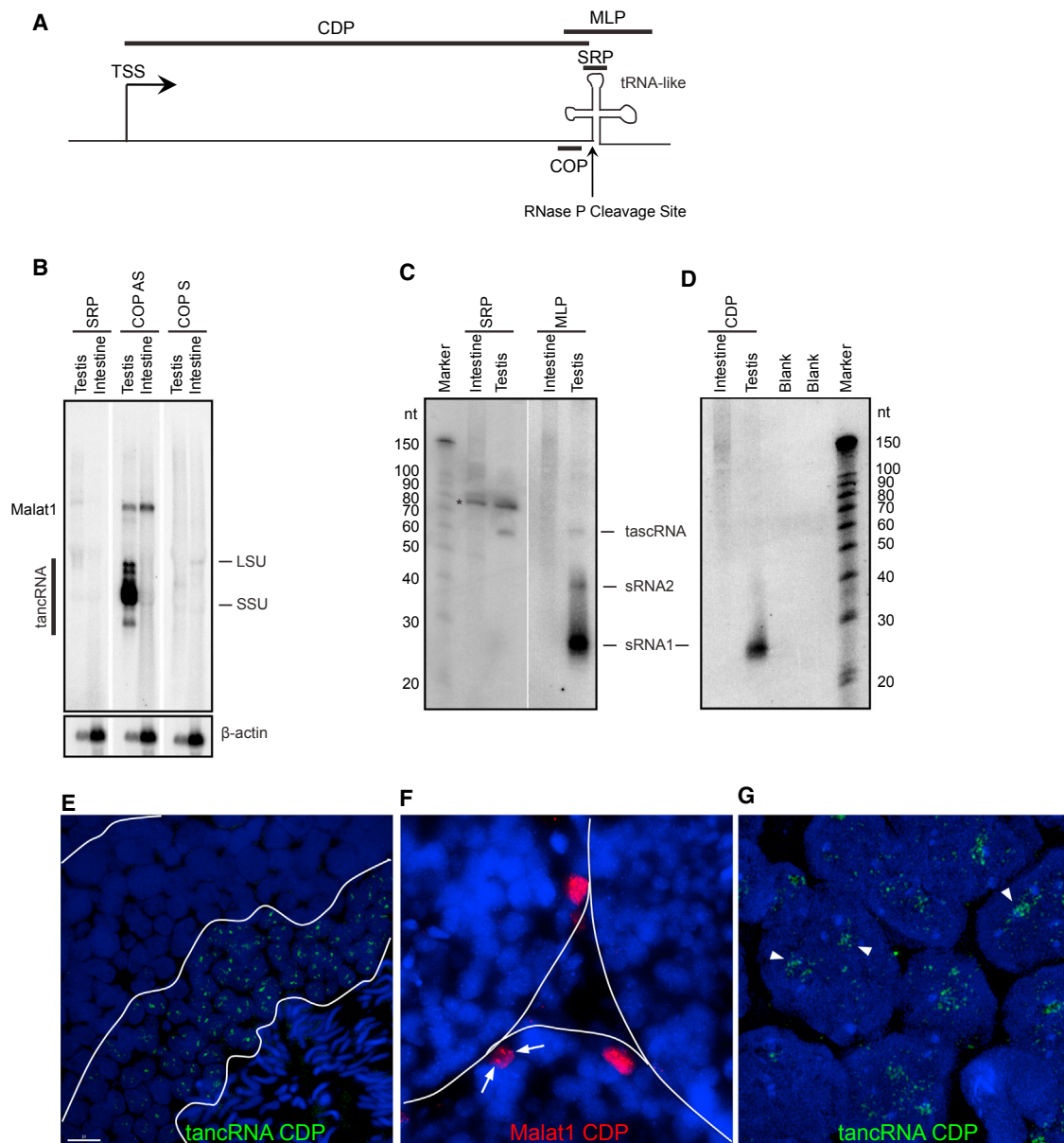


Figure 5. TancRNAs Are Processed and Enriched in Nuclei, and Multiple Small RNA Species Are Produced from TancRNA Loci

(A) Schematic of the transcriptional unit at the *Malat1* 3' module homologous loci. TSS, transcription start site; CDP, cDNA probe (used in D–G); MLP, *MALAT1* 3'-like probe (used in C); the vertical arrow, the predicted RNase P cleavage site just before the tRNA-like structure.

(B) The tancRNAs were processed as human *MALAT1*. Large RNA northern blot analysis shows that SRP (antisense of mascRNA/tancRNA) does not recognize any significant bands (lane 1). COP AS (tancRNA consensus antisense probe) detects both *MALAT1* and tancRNAs (lane 2), while COP S (tancRNA consensus sense probe) does not recognize any significant bands (lane 3).

(C) Multiple small RNA species were produced from tancRNA loci. Small RNA northern blot analysis shows that SRP (mascRNA/tancRNA antisense oligonucleotide probe) detects mascRNA/tancRNA in lizard testis (left), while MLP (consensus PCR-pooled probe) detects three small RNA species with sizes of ~26, 40, and 60 nt (right).

(D) Small RNAs with the size of piRNAs were produced from tancRNA loci. Small RNA northern blot analysis detects a strong RNA band with the size of ~26 nt using CDP (a cDNA probe from the lizard.11 locus; see Data S1).

(E) RNA FISH shows that tancRNAs are localized to nuclei of pachytene and/or round spermatocytes in adult lizard testis.

(F) RNA FISH shows that *MALAT1* is enriched in nuclei of the periphery of seminiferous tubules. Arrows indicate nuclear punctuate signal pattern.

(G) High-resolution imaging of RNA FISH (in E) shows that tancRNAs occupy distinctive nuclear domains (arrowheads). Equal amounts of total RNAs were loaded for each lane. β -actin is the loading control. LSU, large subunit of ribosomal RNA; SSU, small subunit of ribosomal RNA; *non-specific band.

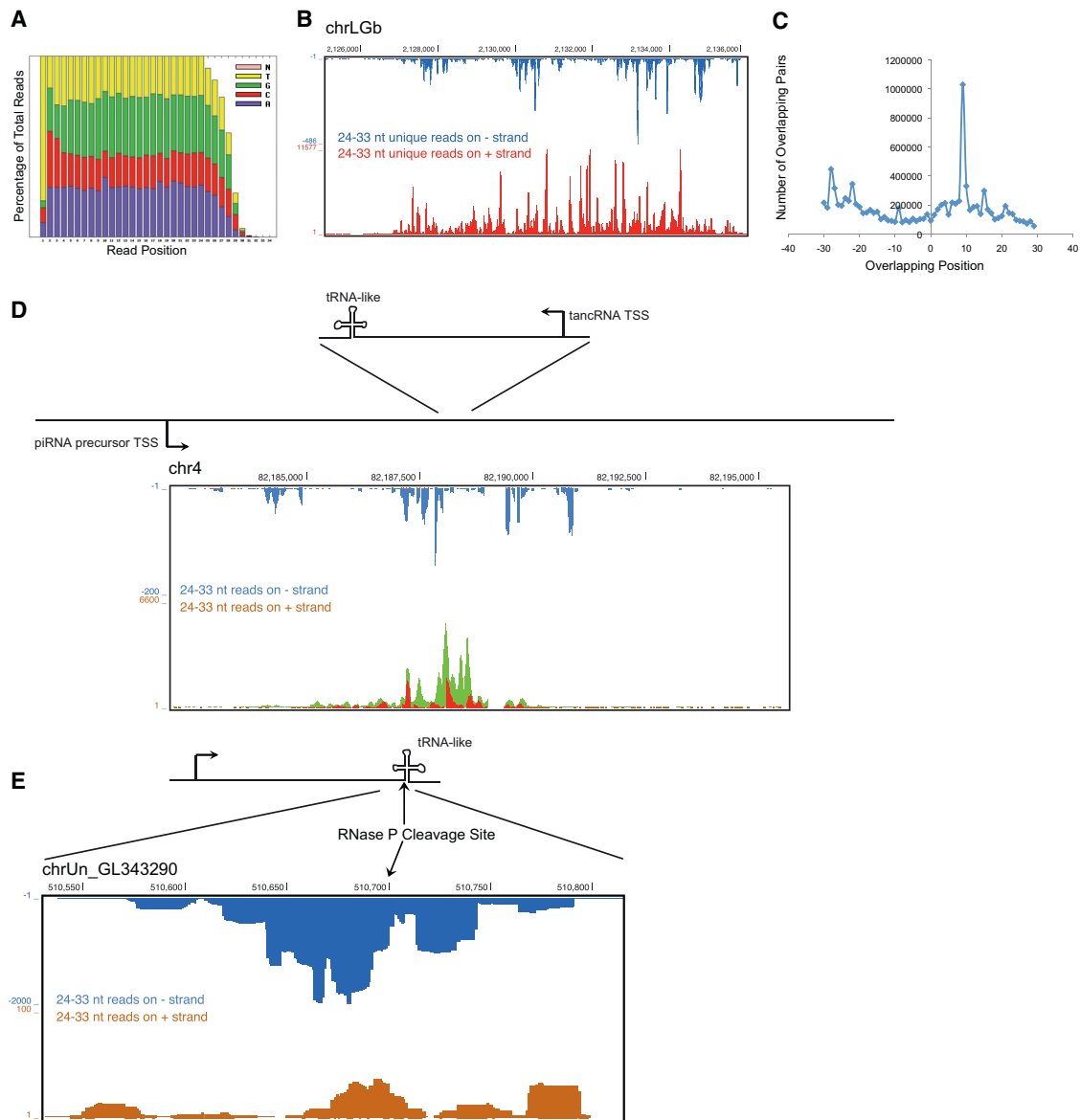


Figure 6. piRNAs Are Produced from the Opposite Strand of TancRNAs

(A) Positional distribution of nucleotide composition of small RNAs sequenced from adult lizard testis. A strong 1U bias and a weak 10A enrichment were noticed. (B) Small RNAs with the size of 24–33 nt were uniquely mapped to a dual-strand piRNA cluster on chrLGB. (C) A strong ping-pong signature of piRNAs from the dual-strand cluster on chrLGB (see B). x axis, overlapping index; y axis, number of overlapping pairs. (D) piRNAs mapped to a tancRNA locus (lizard.37; see [Data S1](#)) on chr4. Orange, unique mapper on negative strand; blue, multiple mapper on negative strand; red, unique mapper on positive strand; green, multiple mapper on positive strand. (E) piRNAs mapped to the 3' end of a tancRNA locus (lizard.2; see [Data S1](#)) on chrUn_GL343290 with multiple mappers (reporting = 50).

of vertebrate lncRNAs with this unique 3' end structural complex. This analysis suggests a role for these RNAs in lizard, and it provides an example to study structure, evolution, and function of lncRNAs.

Chemical probing analysis supports prior studies that demonstrated that the *MALAT1* 3' end module harbors a triple helix with an adjacent hairpin loop, followed by a tRNA-like structure (Brown et al., 2012, 2014; Wilusz et al., 2012). All identified *MALAT1* 3' end homologs in vertebrate genomes encompass

both structural moieties, suggesting that they co-occur. These structures first appeared in jaw-containing vertebrates, produced *NEAT1* lncRNA presumably by gene duplication, and expanded in lizard by an unknown mechanism. However, it is still not clear where this highly structured 3' end module originated. The closest examples are tRNA-like structures (TLSs) in the 3' UTR of the positive strand of plant RNA viruses, which have roles in viral genome replication and translational enhancement. These TLSs are followed by an upstream pseudoknot domain

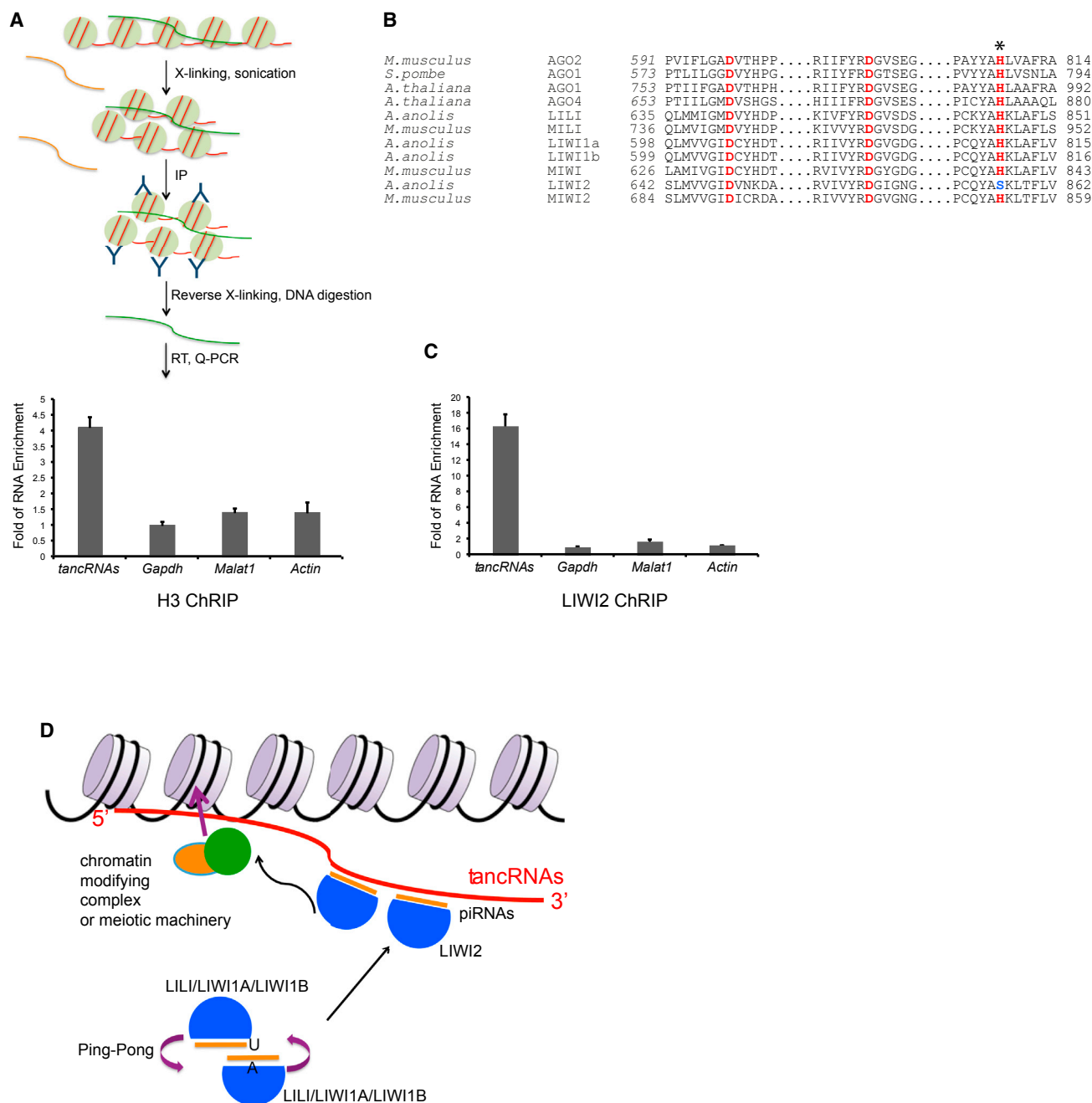


Figure 7. 3' End of TancRNAs Act as Targets of Antisense piRNAs

(A) A schematic diagram of chromatin RNA immunoprecipitation (ChRIP) analysis. ChRIP using antibody against histone H3 shows that tancRNAs (primer sequences in [Data S1](#)) are associated with chromatin.

(B) Sequence alignment showing the catalytic triad (DDH motif) of known Slicers and PIWIs. LIWI2 has a variant of the third His to Ser (H856S; marked with an asterisk).

(C) ChRIP analysis using antibody against LIWI2 shows that tancRNAs are associated with LIWI2. x axis, RNA examined; y axis, fold of RNA enrichment. Sample size n = 3.

(D) A proposed working model of tancRNA-piRNA-LIWI2 complex. TancRNAs act as targets of PIWI-piRNA complexes through their 3' end triplex structure. The 5' end tancRNAs serve as domains to interact with DNA and/or chromatin, therefore tethering PIWI-piRNA complexes to specific genomic loci to regulate chromatin activity.

(UPSK), which also provides translational enhancement (Dreher, 2009). It will be interesting to test if the UPSKs can form a triple helix similar to *MALAT1* and tancRNAs. The discovery of a triple-helix structure in the 3' end of *MALAT1* RNA, the ENE of PAN RNA, and in a pseudoknot structure of Telomerase reverse-transcriptase RNA component (TERC) demonstrates that both viral and eukaryotic organisms utilize the triplex structure for RNA stability and function, respectively (Brown et al., 2012, 2014; Mitton-Fry et al., 2010; Qiao and Cech, 2008; Wilusz et al., 2012). Taken together, the *MALAT1* 3' end represents a unique complex that includes coevolved triple-helix and tRNA-like structures for RNA stability and processing, respectively.

However, several questions remain to be answered. For example, does the triple-helix structure have additional functions besides regulating RNA stability? What is the function of the tRNA-like structure? Does it only provide an RNase P cleavage site to produce lncRNAs with a triple-helix 3' tail? The recent identification of one *MALAT1* triplex-interacting protein, RNA methyltransferase-like protein 16 (METTL16), suggests the existence of a class of triple-stranded RNA-binding proteins (Brown et al., 2016). Future identification of additional proteins associated with the triple-helix and tRNA-like structures will provide further functional insights.

A recent genome-wide bioinformatic search identified ~200 distinct types of ENE-like structures in the intronless transposable element RNAs mostly in plant and fungal genomes (Tycowski et al., 2016). It was postulated that the acquisition of an ENE compensates for the RNA-destabilizing effects of intron loss during transposable element (TE) horizontal transfer (Tycowski et al., 2016). The presence of multiple copies of *MALAT1* 3' end homologs (tancRNAs) in the lizard genome suggests that these genes may behave as transposons and/or their RNA product may have a previously undescribed function. Surprisingly, multiple small RNA species were produced from these loci, including piRNAs from the antisense strand. Despite the high abundance of piRNAs complementary to their 3' ends, tancRNAs are relatively stable. It is unlikely that these tancRNAs serve as cleavage targets for PIWI-piRNA complexes as they are not degraded. The triplex complex may be resistant to PIWI-piRNA cleavage. A second possibility is that the PIWI-piRNA complex-recognizing tancRNAs may not possess enzymatic activity. The latter is indeed supported by the finding that LIWI2 (lizard homolog of MIWI2) is potentially an enzymatically inactive PIWI protein based on in silico protein sequence analysis. Altogether, we propose that tancRNAs act as targets of PIWI-piRNA complexes through their 3' end triplex structure and that 5' end tancRNAs serve as domains to interact with chromatin factors, therefore enabling the tethering of PIWI-piRNA complexes to specifically regulate chromatin activity genome-wide (Figure 7D). Consistent with this hypothesis, human *MALAT1* and *NEAT1* have been shown to associate with the TSSs and gene bodies of active genes in somatic cells (Engreitz et al., 2014; West et al., 2014). We hypothesize that germline-specific lncRNAs with similar function exist in other vertebrate genomes. It will be important to identify and characterize them in order to understand the function of the pachytene piRNA-PIWI complex. For example, a lncRNA has been identified to regulate DNA methylation in *cis* at the im-

printed mouse *Rasgrf1* locus (Davidovich et al., 2013; Watanabe et al., 2011).

In animals, the piRNAs are a class of small silencing RNAs that are generated from piRNA clusters, protect the genome, and may carry out additional yet-to-be-defined functions (Aravin et al., 2006; Aravin and Hannon, 2008; Girard et al., 2006; Grivna et al., 2006; Lau et al., 2006). As new transposons migrate in the genome, they eventually land in piRNA clusters, which generate antisense piRNAs, therefore mediating an immune response against these types of transposons. The unique expansion of tancRNAs in *Anolis carolinensis* led us to speculate that tancRNAs could behave as transposons. Although they are apparently under the control of piRNAs, they are immune to degradation, presumably due to the enzymatically inactive form of LIWI2 or the secondary structure of the 3' end of tancRNAs. Therefore, we propose that tancRNAs not only escaped piRNA-PIWI complex-mediated cleavage but also likely hijacked the complex for chromatin remodeling and/or DNA modification during spermatogenesis.

In mammals, the transposon-silencing response occurs mainly at the embryonic stage, when piRNA clusters are enriched in transposon sequences. However, abundant and transposon-depleted piRNAs produced at pachytene (pachytene piRNAs) are still a mystery (Aravin and Hannon, 2008). RNA-seq analysis of small RNAs from adult *Anolis carolinensis* testis demonstrated that lizard pachytene piRNA clusters have a low content of transposons (B.Z. and D.L.S., unpublished data), but all dual-strand clusters showed a strong ping-pong amplification signature. Moreover, *LIWI2* is highly expressed in adult lizard testis, while *MIWI2* is specifically expressed in embryonic gonads, suggesting unique mechanisms of piRNA biogenesis and action during lizard spermatogenesis. Therefore, adult lizard spermatogenesis may serve as a model to study biogenesis and function of pachytene piRNAs and PIWIs.

In summary, we have defined a class of lncRNAs with coevolved 3' end structures, and we have characterized an acquired function of these RNAs as potential targets of the PIWI-piRNA complex in *Anolis carolinensis*.

EXPERIMENTAL PROCEDURES

All animal protocols have been approved by the Cold Spring Harbor Laboratory (CSHL) Animal Care and Use Committee.

CM Using Infernal

We created a CM using an iterative procedure as follows. Using Infernal v1.1rc1, we built a CM based on the human *MALAT1* 3' end using the cmbuild program, calibrated it for E value reporting with the cmcalibrate program, and searched several vertebrate genomes for high-scoring hits with the cmsearch program. We then aligned those hits to the CM to create a new alignment, filtered that alignment to 92% sequence identity, and built a new CM from the filtered alignment. We repeated this process of building, calibrating, searching, aligning, and filtering for two additional iterations, with some manual refinement of the alignment after each iteration to produce our final CM in the file *MALAT1-3h-tRNAlake.cm* (Data S1) from our final alignment in the file *MALAT1-3h-tRNAlake.stk* (Data S1). Default Infernal v1.1rc1 parameters were used for all steps (cmbuild, cmcalibrate, cmsearch, and cmalign programs).

RNA-Seq Library Preparation

Libraries for deep sequencing were prepared from RNAs extracted from lizard testis and/or brain using TRIzol (Invitrogen), following the long RNA-seq (called

NSR-seq) protocol (Armour et al., 2009) and the standard protocol for small RNAs (He et al., 2012). For NSR-seq, briefly, first-strand cDNA synthesis was performed using SuperScript III (Invitrogen) and the not-so-random forward primer set (5' TCCGATCTCTNNNNNN 3'), followed by second-strand synthesis using exo- Klenow fragment (New England Biolabs) and the not-so-random reverse primer set (5' TCCGATCTGANNNNNN 3'). To deplete rRNAs from the libraries, not-so-random primer sets were designed by pooling 749 unique hexamers with no perfect match to human cytoplasmic 18S and 28S rRNA and mitochondrial 12S and 16S rRNA transcripts. Libraries were subsequently amplified by PCR using primers (5' AATGATACGGCGACCGACGATCTACACTCTTCCCTACACGACGCTCTTCCGATCTCT 3' and 5' CAAGCAGAAGACGGCATACGAGATCGGTCTCGGCATTCTGCTGAACCGCTCTTCCGATCTGA 3') and paired-end sequenced for 50 × 2 cycles on the Illumina Genome Analyzer II, according to the manufacturer's instructions. For small RNA-seq, briefly, RNA was successively ligated to 3' and 5' adaptors, gel purified after each ligation, reverse transcribed, and PCR amplified using Solexa sequencing primers. PCR product was gel purified, quantified, and sequenced for 36 cycles or 76 cycles on the Illumina Genome Analyzer II, according to the manufacturer's instructions.

Sequence Processing, Mapping, and Annotation

For NSR-seq data, the quality of the raw data was evaluated using FastQC (<http://www.bioinformatics.babraham.ac.uk/projects/fastqc/>), and reads were mapped to anoCar2.0 using STAR v2.4.1 (Dobin et al., 2013), resulting in an overall mapping efficiency of 80%. Mapped reads were normalized for read depth as well length, and University of California, Santa Cruz (UCSC) tracks were created using Hypergeometric Optimization of Motif Enrichment (HOMER) (Heinz et al., 2010), allowing for both unique hits and multi-mappers. Parameters were adjusted for strand-specific paired-end sequencing.

For small RNA-seq data, raw reads obtained from the Illumina pipeline were trimmed from 3' linker and filtered for low-quality reads. Unique sequences 24 nt or longer in length were mapped to the anoCar2.0 assembly of the lizard genome using bowtie (<http://bowtie-bio.sourceforge.net/index.shtml>), allowing two mismatches (Langmead et al., 2009).

Northern Blotting Analysis

Northern blots were performed as described previously (Zhang et al., 2012) with minor modifications. Briefly, 10–20 µg RNA longer than 200 nt was resolved by 1% denaturing agarose gel electrophoresis and transferred to Hybond-N membrane (GE Healthcare) by capillary transfer, followed by UV cross-linking. Small RNAs were separated by 15% denaturing PAGE and electrophoretically transferred to Hybond NX membrane (GE Healthcare), followed by 1-ethyl-3-(3-dimethylaminopropyl) carbodiimide cross-linking at 55°C for 1 hr. The cDNA probes (sequence information in Data S1) were labeled with [α -³²P]dCTP using the Prime-It RmT Random Primer Labeling Kit (Stratagene). Oligonucleotide probes (sequence information in Data S1) were labeled with [γ -³²P]ATP using T4 polynucleotide kinase (New England Biolabs). Hybridization was carried out in NorthernMax Prehyb/Hyb Buffer (Ambion) at 42°C for cDNA probes. Hybridization was carried out in ULTRAhyb-Oligo Hybridization Buffer (Ambion) for oligonucleotide probes. Blots were visualized using the Fujifilm Life Science FLA-5100 imaging system.

Other experimental procedures are included in the Supplemental Experimental Procedures.

ACCESSION NUMBERS

The accession number for the sequencing data reported in this paper is GEO: GSE97451.

SUPPLEMENTAL INFORMATION

Supplemental Information includes Supplemental Experimental Procedures, eight figures, and one data file and can be found with this article online at <http://dx.doi.org/10.1016/j.celrep.2017.05.006>.

AUTHOR CONTRIBUTIONS

B.Z., Y.S.M., and D.L.S. conceived and designed all experiments. B.Z. and Y.S.M. performed the experiments. I.V.N. and K.Y.S. planned chemical probing experiments. I.V.N. performed and analyzed chemical probing experiments. C.-S.T. and K.Y.S. planned tertiary structure model. C.-S.T. constructed the model. E.P.N., T.A.J., and S.R.E. performed and analyzed Infernal data. S.D.D. performed RNA-seq analysis. Z.L. performed super-resolution imaging. B.Z., Y.S.M., and W.L. analyzed the data. B.Z., Y.S.M., and D.L.S. wrote the paper with input from all authors.

ACKNOWLEDGMENTS

We thank Carmen Berasain, Jan Bergmann, Megan Bodnar, Melanie Eckersley-Maslin, Stephen Hearn, Ileng Kumaran, Jingjing Li, Cinthya Zepeda-Mendoza, Junwei Shi, and Rui Zhao of the Spector laboratory and Gregory J. Hannon for helpful discussions. We thank Vasily V. Vagin, Yang Yu, Miao He, and Wanhe Li for technical assistance. We acknowledge Los Alamos National Laboratory Directed Research and Development (LDRD). This work was supported by grants from NCI 5P01CA013106-Project 3 and NIGMS 42694 (to D.L.S.). Portions of this study were supported by the Intramural Research Program of the NIH, National Library of Medicine (E.P.N.). B.Z. was supported by a Department of Defense Prostate Cancer Research Program postdoctoral fellowship (W81XWH-10-1-0190). Y.S.M. was supported by a National Cancer Center postdoctoral fellowship. The CSHL Microscopy and DNA Sequencing Shared Resources are supported by NCI 2P30CA45508.

Received: September 7, 2016

Revised: October 27, 2016

Accepted: April 28, 2017

Published: May 23, 2017

REFERENCES

- Aravin, A.A., and Hannon, G.J. (2008). Small RNA silencing pathways in germ and stem cells. *Cold Spring Harb. Symp. Quant. Biol.* 73, 283–290.
- Aravin, A., Gaidatzis, D., Pfeffer, S., Lagos-Quintana, M., Landgraf, P., Iovino, N., Morris, P., Brownstein, M.J., Kuramochi-Miyagawa, S., Nakano, T., et al. (2006). A novel class of small RNAs bind to MILI protein in mouse testes. *Nature* 442, 203–207.
- Armour, C.D., Castle, J.C., Chen, R., Babak, T., Loerch, P., Jackson, S., Shah, J.K., Dey, J., Rohl, C.A., Johnson, J.M., and Raymond, C.K. (2009). Digital transcriptome profiling using selective hexamer priming for cDNA synthesis. *Nat. Methods* 6, 647–649.
- Arun, G., Diermeier, S., Akerman, M., Chang, K.C., Wilkinson, J.E., Hearn, S., Kim, Y., MacLeod, A.R., Krainer, A.R., Norton, L., et al. (2016). Differentiation of mammary tumors and reduction in metastasis upon Malat1 lncRNA loss. *Genes Dev.* 30, 34–51.
- Batista, P.J., and Chang, H.Y. (2013). Long noncoding RNAs: cellular address codes in development and disease. *Cell* 152, 1298–1307.
- Bernard, D., Prasanth, K.V., Tripathi, V., Colasse, S., Nakamura, T., Xuan, Z., Zhang, M.Q., Sedel, F., Jourdain, L., Couplier, F., et al. (2010). A long nuclear-retained non-coding RNA regulates synaptogenesis by modulating gene expression. *EMBO J.* 29, 3082–3093.
- Bertone, P., Stolc, V., Royce, T.E., Rozowsky, J.S., Urban, A.E., Zhu, X., Rinn, J.L., Tongprasit, W., Samanta, M., Weissman, S., et al. (2004). Global identification of human transcribed sequences with genome tiling arrays. *Science* 306, 2242–2246.
- Beyret, E., Liu, N., and Lin, H. (2012). piRNA biogenesis during adult spermatogenesis in mice is independent of the ping-pong mechanism. *Cell Res.* 22, 1429–1439.
- Brown, J.A., Valenstein, M.L., Yario, T.A., Tycowski, K.T., and Steitz, J.A. (2012). Formation of triple-helical structures by the 3'-end sequences of MALAT1 and MEN β noncoding RNAs. *Proc. Natl. Acad. Sci. USA* 109, 19202–19207.

- Brown, J.A., Bulkley, D., Wang, J., Valenstein, M.L., Yario, T.A., Steitz, T.A., and Steitz, J.A. (2014). Structural insights into the stabilization of MALAT1 noncoding RNA by a bipartite triple helix. *Nat. Struct. Mol. Biol.* 21, 633–640.
- Brown, J.A., Kinzig, C.G., DeGregorio, S.J., and Steitz, J.A. (2016). Methyltransferase-like protein 16 binds the 3'-terminal triple helix of MALAT1 long noncoding RNA. *Proc. Natl. Acad. Sci. USA* 113, 14013–14018.
- Budkevich, T.V., Giesebrecht, J., Behrmann, E., Loerke, J., Ramrath, D.J., Mielke, T., Ismer, J., Hildebrand, P.W., Tung, C.S., Nierhaus, K.H., et al. (2014). Regulation of the mammalian elongation cycle by subunit rolling: a eukaryotic-specific ribosome rearrangement. *Cell* 158, 121–131.
- Carninci, P., Kasukawa, T., Katayama, S., Gough, J., Frith, M.C., Maeda, N., Oyama, R., Ravasi, T., Lenhard, B., Wells, C., et al.; FANTOM Consortium; RIKEN Genome Exploration Research Group and Genome Science Group (Genome Network Project Core Group) (2005). The transcriptional landscape of the mammalian genome. *Science* 309, 1559–1563.
- Chodroff, R.A., Goodstadt, L., Sirey, T.M., Oliver, P.L., Davies, K.E., Green, E.D., Molnár, Z., and Ponting, C.P. (2010). Long noncoding RNA genes: conservation of sequence and brain expression among diverse amniotes. *Genome Biol.* 11, R72.
- Davidovich, C., Zheng, L., Goodrich, K.J., and Cech, T.R. (2013). Promiscuous RNA binding by Polycomb repressive complex 2. *Nat. Struct. Mol. Biol.* 20, 1250–1257.
- Derrien, T., Johnson, R., Bussotti, G., Tanzer, A., Djebali, S., Tilgner, H., Guernec, G., Martin, D., Merkel, A., Knowles, D.G., et al. (2012). The GENCODE v7 catalog of human long noncoding RNAs: analysis of their gene structure, evolution, and expression. *Genome Res.* 22, 1775–1789.
- Djebali, S., Davis, C.A., Merkel, A., Dobin, A., Lassmann, T., Mortazavi, A., Tanzer, A., Lagarde, J., Lin, W., Schlesinger, F., et al. (2012). Landscape of transcription in human cells. *Nature* 489, 101–108.
- Dobin, A., Davis, C.A., Schlesinger, F., Drenkow, J., Zaleski, C., Jha, S., Batut, P., Chaisson, M., and Gingeras, T.R. (2013). STAR: ultrafast universal RNA-seq aligner. *Bioinformatics* 29, 15–21.
- Dreher, T.W. (2009). Role of tRNA-like structures in controlling plant virus replication. *Virus Res.* 139, 217–229.
- EiBmann, M., Gutschner, T., Hämmerle, M., Günther, S., Caudron-Herger, M., Groß, M., Schirmacher, P., Rippe, K., Braun, T., Zörnig, M., and Diederichs, S. (2012). Loss of the abundant nuclear non-coding RNA MALAT1 is compatible with life and development. *RNA Biol.* 9, 1076–1087.
- Engreitz, J.M., Sirokman, K., McDonel, P., Shishkin, A.A., Surka, C., Russell, P., Grossman, S.R., Chow, A.Y., Guttman, M., and Lander, E.S. (2014). RNA-RNA interactions enable specific targeting of noncoding RNAs to nascent Pre-mRNAs and chromatin sites. *Cell* 159, 188–199.
- Gilbert, S.D., Rambo, R.P., Van Tyne, D., and Batey, R.T. (2008). Structure of the SAM-II riboswitch bound to S-adenosylmethionine. *Nat. Struct. Mol. Biol.* 15, 177–182.
- Girard, A., Sachidanandam, R., Hannon, G.J., and Carmell, M.A. (2006). A germline-specific class of small RNAs binds mammalian Piwi proteins. *Nature* 442, 199–202.
- Grivna, S.T., Beyret, E., Wang, Z., and Lin, H. (2006). A novel class of small RNAs in mouse spermatogenic cells. *Genes Dev.* 20, 1709–1714.
- Gutschner, T., Hämmerle, M., and Diederichs, S. (2013a). MALAT1 – a paradigm for long noncoding RNA function in cancer. *J. Mol. Med. (Berl.)* 97, 791–801.
- Gutschner, T., Hämmerle, M., Eissmann, M., Hsu, J., Kim, Y., Hung, G., Revenko, A., Arun, G., Stentrup, M., Gross, M., et al. (2013b). The noncoding RNA MALAT1 is a critical regulator of the metastasis phenotype of lung cancer cells. *Cancer Res.* 73, 1180–1189.
- Guttman, M., Amit, I., Garber, M., French, C., Lin, M.F., Feldser, D., Huarte, M., Zuk, O., Carey, B.W., Cassady, J.P., et al. (2009). Chromatin signature reveals over a thousand highly conserved large non-coding RNAs in mammals. *Nature* 458, 223–227.
- Harrow, J., Frankish, A., Gonzalez, J.M., Tapanari, E., Diekhans, M., Kokocinski, F., Aken, B.L., Barrell, D., Zadissa, A., Searle, S., et al. (2012). GENCODE: the reference human genome annotation for The ENCODE Project. *Genome Res.* 22, 1760–1774.
- He, M., Liu, Y., Wang, X., Zhang, M.Q., Hannon, G.J., and Huang, Z.J. (2012). Cell-type-based analysis of microRNA profiles in the mouse brain. *Neuron* 73, 35–48.
- Heinz, S., Benner, C., Spann, N., Bertolino, E., Lin, Y.C., Laslo, P., Cheng, J.X., Murre, C., Singh, H., and Glass, C.K. (2010). Simple combinations of lineage-determining transcription factors prime cis-regulatory elements required for macrophage and B cell identities. *Mol. Cell* 38, 576–589.
- Hutchinson, J.N., Ensminger, A.W., Clemson, C.M., Lynch, C.R., Lawrence, J.B., and Chess, A. (2007). A screen for nuclear transcripts identifies two linked noncoding RNAs associated with SC35 splicing domains. *BMC Genomics* 8, 39.
- Ji, P., Diederichs, S., Wang, W., Böing, S., Metzger, R., Schneider, P.M., Tidow, N., Brandt, B., Buerger, H., Bulk, E., et al. (2003). MALAT-1, a novel noncoding RNA, and thymosin beta4 predict metastasis and survival in early-stage non-small cell lung cancer. *Oncogene* 22, 8031–8041.
- Kang, M., Eichhorn, C.D., and Feigon, J. (2014). Structural determinants for ligand capture by a class II preQ1 riboswitch. *Proc. Natl. Acad. Sci. USA* 111, E663–E671.
- Kapranov, P., Willingham, A.T., and Gingeras, T.R. (2007). Genome-wide transcription and the implications for genomic organization. *Nat. Rev. Genet.* 8, 413–423.
- Katayama, S., Tomaru, Y., Kasukawa, T., Waki, K., Nakanishi, M., Nakamura, M., Nishida, H., Yap, C.C., Suzuki, M., Kawai, J., et al.; RIKEN Genome Exploration Research Group; Genome Science Group (Genome Network Project Core Group); FANTOM Consortium (2005). Antisense transcription in the mammalian transcriptome. *Science* 309, 1564–1566.
- Kuhn, C.D., Wilusz, J.E., Zheng, Y., Beal, P.A., and Joshua-Tor, L. (2015). On-enzyme refolding permits small RNA and tRNA surveillance by the CCA-adding enzyme. *Cell* 160, 644–658.
- Langmead, B., Trapnell, C., Pop, M., and Salzberg, S.L. (2009). Ultrafast and memory-efficient alignment of short DNA sequences to the human genome. *Genome Biol.* 10, R25.
- Lau, N.C., Seto, A.G., Kim, J., Kuramochi-Miyagawa, S., Nakano, T., Bartel, D.P., and Kingston, R.E. (2006). Characterization of the piRNA complex from rat testes. *Science* 313, 363–367.
- Lee, S., Kopp, F., Chang, T.C., Sataluri, A., Chen, B., Sivakumar, S., Yu, H., Xie, Y., and Mendell, J.T. (2016). Noncoding RNA NORAD Regulates Genomic Stability by Sequestering PUMILIO Proteins. *Cell* 164, 69–80.
- Limmer, S., Hofmann, H.P., Ott, G., and Sprinzl, M. (1993). The 3'-terminal end (NCCA) of tRNA determines the structure and stability of the aminoacyl acceptor stem. *Proc. Natl. Acad. Sci. USA* 90, 6199–6202.
- Mao, Y.S., Sunwoo, H., Zhang, B., and Spector, D.L. (2011). Direct visualization of the co-transcriptional assembly of a nuclear body by noncoding RNAs. *Nat. Cell Biol.* 13, 95–101.
- Mitton-Fry, R.M., DeGregorio, S.J., Wang, J., Steitz, T.A., and Steitz, J.A. (2010). Poly(A) tail recognition by a viral RNA element through assembly of a triple helix. *Science* 330, 1244–1247.
- Nakagawa, S., Ip, J.Y., Shioi, G., Tripathi, V., Zong, X., Hirose, T., and Prasanth, K.V. (2012). Malat1 is not an essential component of nuclear speckles in mice. *RNA* 18, 1487–1499.
- Nawrocki, E.P., and Eddy, S.R. (2013). Infernal 1.1: 100-fold faster RNA homology searches. *Bioinformatics* 29, 2933–2935.
- Okazaki, Y., Furuno, M., Kasukawa, T., Adachi, J., Bono, H., Kondo, S., Nikaide, I., Osato, N., Saito, R., Suzuki, H., et al.; FANTOM Consortium; RIKEN Genome Exploration Research Group Phase I & II Team (2002). Analysis of the mouse transcriptome based on functional annotation of 60,770 full-length cDNAs. *Nature* 420, 563–573.

- Ørom, U.A., Derrien, T., Beringer, M., Gumireddy, K., Gardini, A., Bussotti, G., Lai, F., Zytznicki, M., Notredame, C., Huang, Q., et al. (2010). Long noncoding RNAs with enhancer-like function in human cells. *Cell* 143, 46–58.
- Pauli, A., Valen, E., Lin, M.F., Garber, M., Vastenhouw, N.L., Levin, J.Z., Fan, L., Sandelin, A., Rinn, J.L., Regev, A., and Schier, A.F. (2012). Systematic identification of long noncoding RNAs expressed during zebrafish embryogenesis. *Genome Res.* 22, 577–591.
- Qiao, F., and Cech, T.R. (2008). Triple-helix structure in telomerase RNA contributes to catalysis. *Nat. Struct. Mol. Biol.* 15, 634–640.
- Rinn, J.L., and Chang, H.Y. (2012). Genome regulation by long noncoding RNAs. *Annu. Rev. Biochem.* 81, 145–166.
- Rinn, J.L., Kertesz, M., Wang, J.K., Squazzo, S.L., Xu, X., Bruggmann, S.A., Goodnough, L.H., Helms, J.A., Farnham, P.J., Segal, E., and Chang, H.Y. (2007). Functional demarcation of active and silent chromatin domains in human HOX loci by noncoding RNAs. *Cell* 129, 1311–1323.
- Shevtsov, S.P., and Dundr, M. (2011). Nucleation of nuclear bodies by RNA. *Nat. Cell Biol.* 13, 167–173.
- Song, J.J., Smith, S.K., Hannon, G.J., and Joshua-Tor, L. (2004). Crystal structure of Argonaute and its implications for RISC slicer activity. *Science* 305, 1434–1437.
- Stadler, P.F. (2010). Evolution of the Long Non-coding RNAs MALAT1 and MEN β /ε. C.E. Ferreira, S. Miyano, and P.F. Stadler, eds. *Proceedings of the Fifth Brazilian Symposium on Bioinformatics: Advances in Bioinformatics and Computational Biology* 6268, 1–12.
- Tripathi, V., Ellis, J.D., Shen, Z., Song, D.Y., Pan, Q., Watt, A.T., Freier, S.M., Bennett, C.F., Sharma, A., Bubulya, P.A., et al. (2010). The nuclear-retained noncoding RNA MALAT1 regulates alternative splicing by modulating SR splicing factor phosphorylation. *Mol. Cell* 39, 925–938.
- Tung, C.S., Joseph, S., and Sanbonmatsu, K.Y. (2002). All-atom homology model of the Escherichia coli 30S ribosomal subunit. *Nat. Struct. Biol.* 9, 750–755.
- Tycowski, K.T., Shu, M.D., and Steitz, J.A. (2016). Myriad Triple-Helix-Forming Structures in the Transposable Element RNAs of Plants and Fungi. *Cell Rep.* 15, 1266–1276.
- Ullitsky, I., and Bartel, D.P. (2013). lincRNAs: genomics, evolution, and mechanisms. *Cell* 154, 26–46.
- Ullitsky, I., Shkumatava, A., Jan, C.H., Sive, H., and Bartel, D.P. (2011). Conserved function of lincRNAs in vertebrate embryonic development despite rapid sequence evolution. *Cell* 147, 1537–1550.
- Watanabe, T., Tomizawa, S., Mitsuya, K., Totoki, Y., Yamamoto, Y., Kuramochi-Miyagawa, S., Iida, N., Hoki, Y., Murphy, P.J., Toyoda, A., et al. (2011). Role for piRNAs and noncoding RNA in de novo DNA methylation of the imprinted mouse Rasgrf1 locus. *Science* 332, 848–852.
- West, J.A., Davis, C.P., Sunwoo, H., Simon, M.D., Sadreyev, R.I., Wang, P.I., Tolstorukov, M.Y., and Kingston, R.E. (2014). The long noncoding RNAs NEAT1 and MALAT1 bind active chromatin sites. *Mol. Cell* 55, 791–802.
- Wilusz, J.E., Freier, S.M., and Spector, D.L. (2008). 3' end processing of a long nuclear-retained noncoding RNA yields a tRNA-like cytoplasmic RNA. *Cell* 135, 919–932.
- Wilusz, J.E., Whipple, J.M., Phizicky, E.M., and Sharp, P.A. (2011). tRNAs marked with CCACCA are targeted for degradation. *Science* 334, 817–821.
- Wilusz, J.E., JnBaptiste, C.K., Lu, L.Y., Kuhn, C.D., Joshua-Tor, L., and Sharp, P.A. (2012). A triple helix stabilizes the 3' ends of long noncoding RNAs that lack poly(A) tails. *Genes Dev.* 26, 2392–2407.
- Yang, L., Lin, C., Liu, W., Zhang, J., Ohgi, K.A., Grinstein, J.D., Dorrestein, P.C., and Rosenfeld, M.G. (2011). ncRNA- and Pc2 methylation-dependent gene relocation between nuclear structures mediates gene activation programs. *Cell* 147, 773–788.
- Zhang, B., Arun, G., Mao, Y.S., Lazar, Z., Hung, G., Bhattacharjee, G., Xiao, X., Booth, C.J., Wu, J., Zhang, C., and Spector, D.L. (2012). The lncRNA Malat1 is dispensable for mouse development but its transcription plays a cis-regulatory role in the adult. *Cell Rep.* 2, 111–123.